FINISAR

Application Note AN-2133

High Speed Characteristics of VCSELs

First published in Proceedings of the SPIE, vol. 3004

ABSTRACT

The high speed characteristics of Vertical Cavity Surface Emitting Lasers (VCSELs) for use in modern high bandwidth fiber optic networks is presented. An equivalent circuit model based on microwave network analyzer S 11 measurements is developed. The dynamic operation of multi-transverse mode VCSELs is also investigated. Experimentally, a laser with two orthogonally polarized modes is examined. We show that each of the transverse laser modes may have significantly different rise and fall times. A multimode rate equation model is used to predict the exact pulseshape for each mode. The laser gain is saturated by the total optical intensity, and the sum of the modal powers is shown to have a constant rise and fall time. The system performance in terms of the bit error rate is also investigated. We demonstrate that selective attenuation of the optical modes can lead to an increase in the bit error rate due to polarization partitioning noise.

INTRODUCTION

The Vertical Cavity Surface Emitting Laser (VCSEL) is emerging as the light source of choice for modern high speed, short wavelength communication systems. The inherent low cost of manufacture [1], enhanced reliability [2], nonastigmatic and circularly symmetric optical output are among the advantages of VCSELs over traditional edge emitting lasers. However much of the development and characterization performed on edge emitting devices must be reexamined for use with the VCSEL. For edge emitting lasers typically used in short wavelength telecommunication applications, there has been a vast amount of work done to ensure stable single transverse mode emission, and in some cases single longitudinal mode operation. Single transverse mode operation increases the efficiency of coupling light into a fiber optic cable, and the low longitudinal mode count significantly reduces chromatic dispersion in the fiber. In VCSEL emission, the output is typically multi-transverse mode and single longitudinal mode. The total spectral width of the emission is generally less than 5 Angstroms, which ensures a low coherence source, but not at the expense of chromatic dispersion. The circularly symmetric and non astigmatic emission of the VCSEL, even in multi-transverse modes, typically has a beam divergence angle less than 12° FWHM (NA=0.12). This easily couples into high NA (0.275) multimode (62.5/125 mm) graded index fiber generally found in LAN backbones. The narrow beam emission is set by the coupling of the mode to the Bragg grating, and for high contrast gratings, the mode size is reduced and the emission angle is increased. Finally, the surface emitting structure and small mode size enables production of highly uniform and densely packed lasers, with minimal crosstalk, for use in parallel optical links.

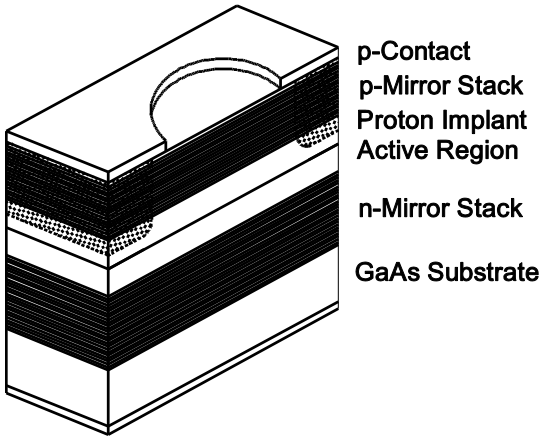

Figure 1. Schematic of a VCSEL.

The lasers used in this work were grown by low pressure MOCVD, and designed to emit at 850nm [2,3]. The structure is shown schematically in Fig. 1. The p-mirror stack consists of 20.5 periods of alternating layers of AlAs/$Al_{0.15}Ga_{0.85}As$. The active region contains three GaAs quantum wells surrounded by $Al_{0.25}Ga_{0.75}As$ spacers, and the cavity is spaced to form a single wavelength cavity with $Al_{0.6}Ga_{0.4}As$. The n-mirror consists of 22.5 periods of AlAs/$Al_{0.15}Ga_{0.85}As$ pairs grown on an n-type GaAs substrate. Current confinement was achieved by proton implantation. The VCSEL is intended for commercial use and has an inner diameter of 20 mm and a top metal aperture of 15mm. This provides the best balance of threshold current, modulation bandwidth, series resistance and spectral width. Typical forward voltage and light output versus current relationship for ambient temperatures of 10, 40 and 70°C are shown in Fig. 2. The laser threshold current is stable within 1mA over approximately 80°C temperature variation. This allows VCSELs to be used in an open loop driving circuit, significantly reducing the cost. The forward operating voltage is typically 1.8V with a series resistance of 20 Ohms, enabling the VCSEL to be driven directly with low voltage sources and PECL/ECL logic. Typical slope efficiencies are 0.2mW/mA.

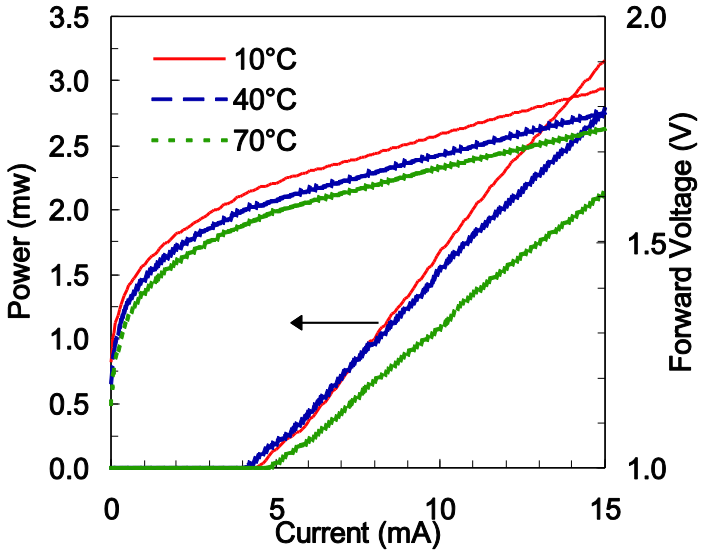

Figure 2. Typical LIV curves for 10, 40 and 70C.

EQUIVALENT CIRCUIT PARAMETERS

The equivalent lumped circuit model of a VCSEL is of great practical utility to design interface drive circuits for high speed modulation. To measure the impedance of a VCSEL, packaging parasitics were minimized by uising silver epoxy to mount a VCSEL on a copper circuit board. Electrical contact was made via a wire bond attached to a 50 ohm custom ceramic stripline. The stripline was electrically contacted through a high speed microwave probe. The stripline and the probe have a bandwidth in excess of 20Ghz. A network analyzer, calibrated to the end of the microstrip line by use of an identical ceramic standard, was used to measure the reflection (S_{11}) coefficient as a function of frequency and dc bias current. To ensure the VCSEL was being modulated in the small signal regime, the input electrical power was kept under -40dBm. The circuit model appropriate for subthreshold bias currents is shown in Fig. 3.

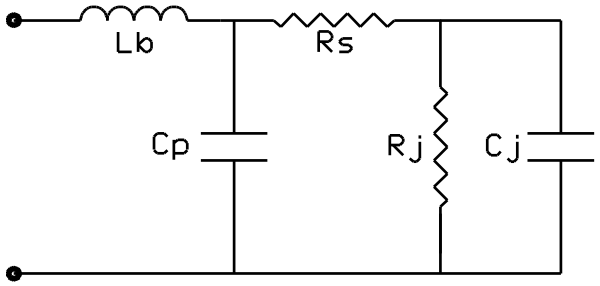

Figure 3 VCSEL Equivalent circuit

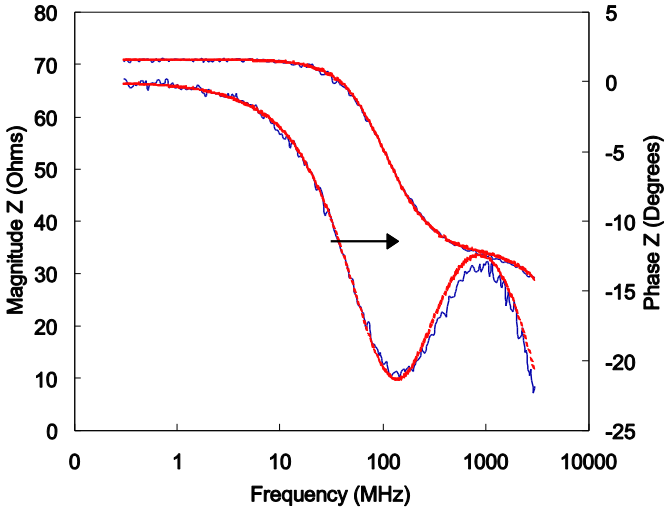

Figure 4. Measured and calculated VCSEL impedance

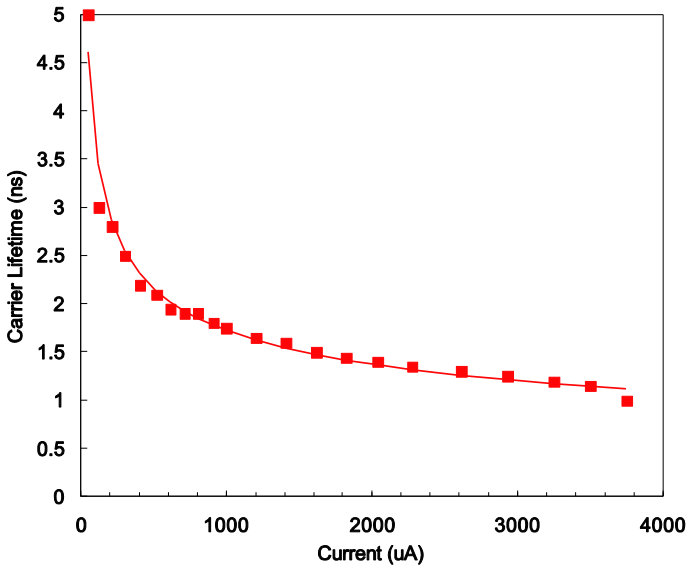

Figure 5. Measured differential carrier lifetime and fit.

The components that make up the equivalent circuit include an inductance Lb due to the bond wire, a capacitance Cp from the VCSEL chip, and a resistance Rs arising from the metal contacts and the resistance of the Bragg mirror stack. The p-n junction is modeled by a capacitance Cj and a resistance R j in parallel. The differential carrier lifetime is given by td=RjCj. The measured VCSEL impedance magnitude and phase, for a bias current of 1 mA, is shown in Fig. 4 as the solid lines. The fit obtained using our model is indicated as the broken lines in Fig. 4, and the values of the components are L b=0.25nH, Cp=0.8pF, Rs=35W, and td=1.75ns. At low frequencies, the VCSEL

impedance is real, and is giving by the sum of R s and Rj. As the frequency increases, the junction capacitance dominates, and the real part of the impedance reduces to R s. Excellent agreement between the VCSEL and its equivalent circuit are obtained over a very large range of operating temperatures and currents, indicating the appropriateness of our model. Figure 5 shows the measured differential carrier lifetime calculated from the impedance measurements as described in [4]. This all electrical technique yields much more accurate results than the commonly used optical techniques, particularly at the low bias currents associated with VCSEL operation. Accurate carrier lifetime measurements allow for a proper estimation of the threshold carrier density, which in turn enables estimation of non-radiative recombination processes. The solid line in Fig. 5 is a fit to the measured carrier lifetime as a function of the dc bias current. We find the carrier lifetime can be approximated by:

$$\tau_d \cong 0.033 + \frac{16.85}{\sqrt[3]{I}}$$

where I is the injected current in μA, and τd is in ns. The total carrier density in the active region is then found by integrating the current times the carrier lifetime,

$$n(I) = \int_0^I \tau_d(I')\,dI'$$

yielding a threshold carrier density of 2 ´10^{18} cm^{-3}. Using traditional optical techniques for carrier density measurements, we would have overestimated the threshold carrier density by about 40%. The simple equivalent circuit model described here can be used to quite accurately model the laser impedance for design into communication systems. In addition, the correct carrier lifetime measurements allow the optical designer to better understand the mechanics of the laser itself.

$$\Delta\nu_{coh} = \frac{\left[\int S(\nu)d\nu\right]^2}{\int S^2(\nu)d\nu}$$

MULTI-TRANSVERSE MODE OPERATION

In contrast to edge emitting lasers, the orientation of the quantum well active region with respect the Bragg mirrors causes little polarization selection of the optical output of a VCSEL, and the emission tends to be polarized along the

[1 1 0] / [110] crystallographic axes. This has recently been shown to be caused by a small anisotropy in the elastic lattice tensor [5]. Because of the small anisotropy and a polarization independent gain, the optical modes of a VCSEL are essentially randomly polarized between the two orthogonal [110] and [1 1 0] crystallographic planes. Using spectroscopically and polarization resolved near field emission, complete families of both Laguerre-Gaussian and Hermite-Gaussian optical modes have been shown to exist in VCSELs [6]. These multiple transverse modes, each with a different wavelength, help deco-here the laser source and thus make it less susceptible to

interference effects, such as fiber modal noise, in communication systems. In Fig. 6 is a plot of the coherence of a VCSEL as a function of the dc current.

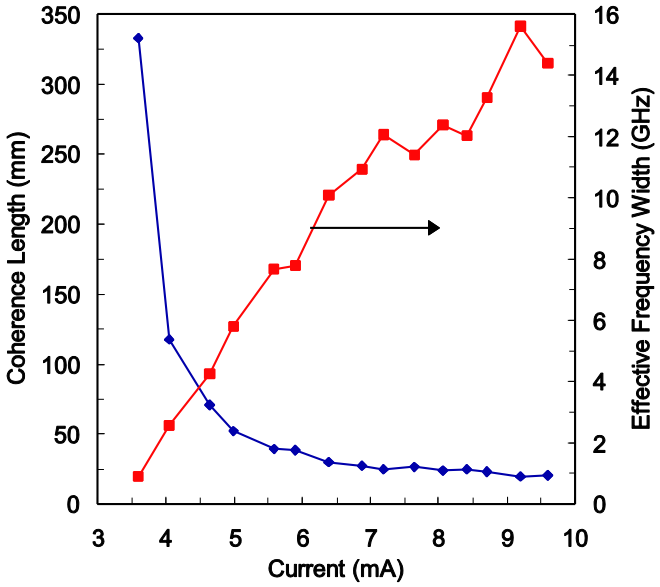

Figure 6 Coherence length and effective frequency width of a VCSEL.

The coherence was calculated using:

where S(n) is the photon density at frequency n. The optical frequency spectrum at threshold, 3.5mA, was nearly single frequency , with a second frequency component appearing at 4.5mA. Typical spectral linewidths were less than 1 Ghz. At high bias currents, I>5mA, there are at least 5 independent frequency components evident in the optical spectrum. These spectral components were found to tune at 0.065nm/°C and 0.083nm/mA. (This gives a junction temperature rise of 1.27°C/mA.) It is important to note the total spectral band-width is still less than 5 because the laser is multi-transverse mode. The longitudinal mode spacing of the VCSEL is about 40nm. Each of the transverse modes has its wave vector oriented at an angle with respect to the emission direction, and the mode wavelength is defined by the projection of the wave vector onto the optical axis. This projection leads to the small differences in wavelength observed for each transverse mode [6,7]. Since each of the transverse modes may be polarized along either the [110] or the [1 1 0] crystallographic planes, polarizing components in the optical path could severely limit VCSEL performance in an optical system. As an illustration, the per cent power in each of the two orthogonal modes is plotted as a function of the dc bias current in Fig. 7. We have arbitrarily labeled the [110] direction P, and the [1 1 0] direction S polarization. As the dc bias current is increased, the laser polarization is seen to switch between the S and P polarizations. Recently there have been several attempts by researchers to control the polarization state by introducing anisotropy in

either the geometry [8,9] or gain [10,11]. These have met with varying degrees of success, and the impact on device reliability is unknown.

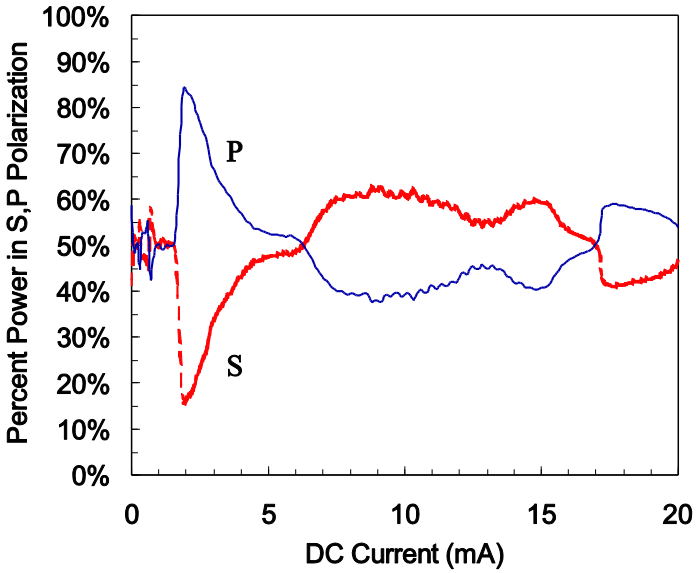

Figure 7 Percent power in the S and P modes of a VCSEL.

The non-degeneracy of the transverse mode family both spatially and in polarization may lead to a reduction in coherence of the laser, but it also creates some interesting effects when selective modal attenuation mechanisms act on the laser output field. Selective modal attenuation can be manifested in a number of ways. Polarization selective elements may occur in components of the fiber link such as beamsplitters, fused couplers, diffractive lenses etc, each of which may differentially attenuate modes depending on their polarization state. In the worst case, they may completely block one mode and pass the other unattenuated. Modes may be selectively spatially attenuated when coupling into fibers or passing through spatially inhomogeneous optical elements. In particular, overfilled launches into optical fibers or vignetting of beams through aperture stops will tend to select modal fields in the center of the VCSEL and block modes nearer the outer perimeter. In some VCSEL designs modes may even lase under the contact ring, preventing the optical power of those modes from leaving the laser.

The effects of selective modal attenuation fall into three broad categories. First there is Bit Error Rate (BER) degradation due to selection induced turn-on jitter [12], secondly there are pulse distortion effects [13], and thirdly there is BER degradation due to selection induced mode partition noise. All of these effects have the same root cause, namely that the distribution of power between the lasing modes changes with time even when the total power emitted from the laser appears to have reached steady state saturation [14]. If one of these modes is preferentially selected, the

effects of the mode competition will then become evident as jitter; as mode partition amplitude noise; or as long time constant tailing effects on the rising edge of the optical pulse.

The effect of polarization selectivity on turn-on delay induced jitter on the rising edge was investigated by Kuksenkov et al. [12]. In their case, the polarization selectivity was introduced by breaking the degeneracy of the polarization eigenmodes in the laser itself. This was accomplished by designing a polarization controlling structure that created enough differential gain between the eigenmodes to allow one of them to become the dominant mode. However, due to spontaneous emission, there is a finite probability that under transient conditions the laser may start to lase in the secondary mode and quickly switch to the dominant mode. This would create distortion on the rising edge due to the different gains of the modes, and would be present on some pulses but not on others. This alone would not cause turn-on jitter. However, if an external polarization selective element was also present, then the secondary mode would be blocked entirely and this effect would create turn-on delay jitter in addition to distortion on the rising edge. Even when the total power of the modes reaches steady state due to gain saturation of the optical power, the individual modes of the laser may still be competing with each other for the gain, and may not have reached steady state. Lam et al. showed from a study of the multimode rate equations in multi-longitudinal mode quantum well edge emitters that the individual modes may take more than five times longer to reach steady state than the total power [14]. In the case of a single transverse mode edge emitter, all the modes clearly compete for the same gain, because they occupy essentially the same mode volume. Consequently there is no mechanism where the individual modes can be selectively observed by spatial or polarization means. The long settling times of the individual modes are typically not observed in edge emitters, and it is only possible to observe the sum of the power of all the modes. In multi-transverse mode VCSELs however, the modes can be spatially selected or selected by polarization as described above.

In this section we examine the effect of polarization selection of modes on pulse rise times by studying the simple case of a two moded VCSEL where the modes have orthogonal polarizations. The modes have a strong spatial overlap, and thus compete for the same gain. This allows us to invoke a simple multimode rate equation model, with no spatially dependent terms, to explain the observed effects.

In order to facilitate testing in fiber networks, a VCSEL was mounted on a transistor TO46 header and placed on a large thermoelectrically controlled heat sink. A bias tee was employed to allow both a dc biasing current and an ac modulation current. The laser was collimated using a 0.12 NA lens, closely matching the VCSEL emission. The laser was operated in a multi-transverse mode, and we were able to separate the orthogonal modes using a polarizer. In addition to the fiber network, the light was directed to an average power detector; an avalanche photodiode; or a Fabry-Perot interferometer. To verify the number of modes operating both near field images and spectral characteristics were measured.

$$\frac{dN_2}{dt} = \frac{-1}{\tau_2}\left[N_2 - P(t) + (N_2 - N_1)\sum_j \Gamma_j I_j\right]$$

$$\frac{dN_1}{dt} = \frac{-1}{\tau_2}\left[N_1\frac{\tau_2}{\tau_1} - N_1 - (N_2 - N_1)\sum_j \Gamma_j I_j\right]$$

$$\frac{dI_j}{dt} = \frac{-1}{\tau_c}\left[\Gamma_j I_j - \beta_j(N_2 - N_1) - (N_2 - N_1)\sum_j \Gamma_j I_j\right]$$

By selectively eliminating one of the modes, we were able to look at the individual modal dependent rise and fall times, and the individual pulse shapes. The solid lines in Figs. 8, 9, and 10 are the modal dependent pulse shapes for the polarizer at 0°, +45°, and -45° respectively. There are clearly three very distinct pulse shapes associated with the modes. With the polarizer at 0°, each of the modes is transmitted equally, corresponding to the total optical power output, and the pulseshape is rectangular with approximately 100ps detector limited 20%-80% rise and fall times. The “bounce” in the off state of the laser is caused by diffusion of carriers into the lasing mode from the non lasing background volume [15]. When the polarizer is rotated to +45°, one of the lasing modes is eliminated, and a very fast rise time of 100ps is observed, and an exponential decay to steady state is observed with an approximately 1ns time constant. This yields an effective fall time for the mode of about 1.5ns. (The turn off of the electrical pulse occurs before the output has reached steady state.) Conversely, when the polarizer is rotated to -45°, the output has a very slow rise time of 1.5ns, and a fast fall time of 100ps. It should be noted in the case where the polarizer passes the modes with equal weighting (0 degree position), corresponding to the transmission of the total power, the pulse is not distorted and the settling time is dominated by the laser relaxation oscillation.

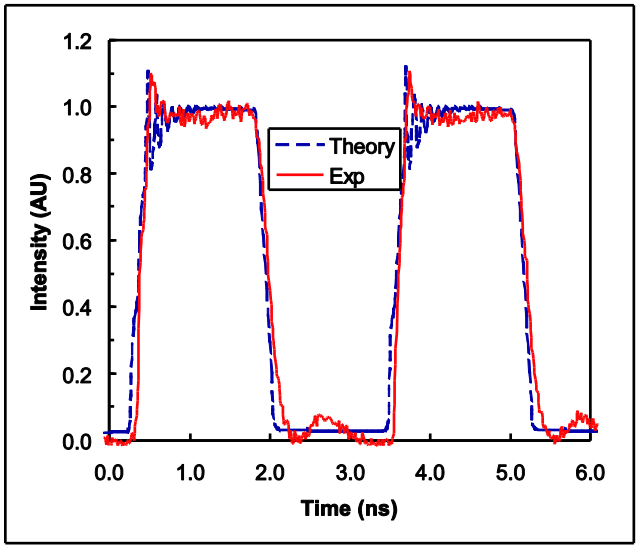

Figure 8. Output from the VCSEL with the polarizer at 0 degrees.

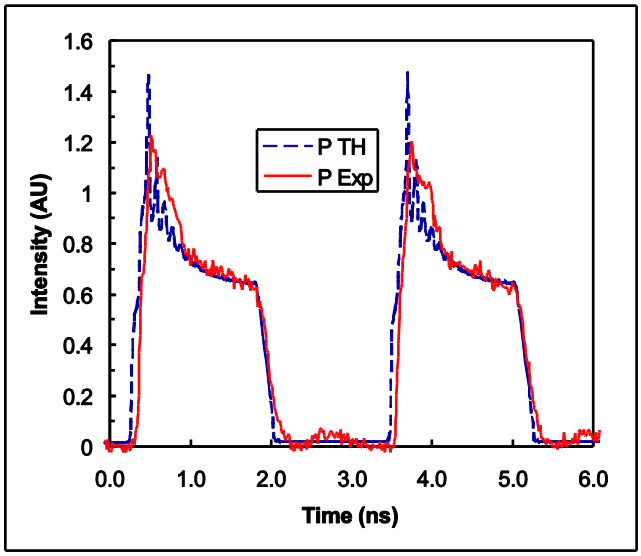

Figure 9. Output from the VCSEL with the polarizer at +45 degrees.

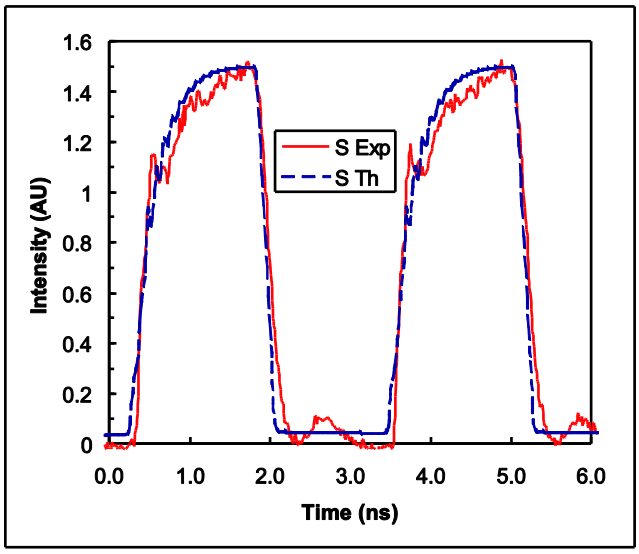

Figure 10. Output from the VCSEL with the polarizer at -45 degrees.

However, when the polarizer is oriented to select only one mode, the pulse shape is severely distorted and the settling time is very long, and is dominated by mode competition effects rather than the relaxation oscillation. It is intuitively obvious that if some modes appear to overshoot and then relax back to the steady state value, others will undershoot and have a long rise time. Because the gain saturates as the total intensity, the sum of the two, will exactly compensate each other. In a real world case where the polarization selection may be partial, the pulse will simply appear to have a slow tail or an overshoot on the rising edge. The exact pulseshape will depend on what degree

the above compensation has been compromised by differentially removing some of the power from the modes. This effect is likely to cause power penalties due to pulse distortion in a real optical link.

In order to develop an understanding of the possible implications to VCSEL performance in modulation experiments, we have employed a multimode rate equation model. The rate equations, normalized to their steady state values, are given by;

where N_1 is the number of electrons in the valence band, N_2 is the number of electrons in the conduction band, P(t) is the injected carrier density, and I_j is the intensity of the j^{th} mode.

All of these values are normalized to the steady state characteristics in order to facilitate computer modeling. The time constants in equations (1) - (3) are the spontaneous emission lifetime τ_2 (1ns), the hole lifetime τ_1 (1ps), and the photon lifetime τ_c (4ps). The coupling of spontaneous emission to the j^{th} lasing mode is β_j, and the mode overlap with the gain region is G_j. It is important to note the gain in the above equation is saturated by the total optical intensity and there are no lateral carrier diffusion effects. It has been shown by other researchers that spatial hole burning of the Laguerre-Gaussian modes can lead to mode competition and modal dependent rise times [15,16]. The rate equations were solved for 2 independent modes subjected to a dc offset digital input. The analysis can be easily extended to include an arbitrary number of modes. The results of our simulation are shown as the dashed lines in Figs. 8, 9, and 10. Figure 8 shows how the total intensity, or the sum of the two modes evolves in time. Figures 9 and 10 show how the individual modes evolve in time. Excellent agreement between theory and experiment is achieved without using a spatial dependent carrier concentration. At high output power, or for many lateral modes, it may become important to include lateral carrier diffusion in the rate equations [15]. In addition, to model lasers that do not have large overlap of the individual optical modes, as in the case of filamentary large aperture VCSELs, it may be necessary to include carrier diffusion and mode competition in the laser rate equations. For many cases, simple mode competition will suffice as a model because the physical size of the spatial modes are of the same order, and the numerical aperture of the modes is effectively limited by the Bragg reflector. The large overlap of each of the modes encourages mode competition, saturation of the gain by the total optical intensity, and our simple rate equation is applicable. We have shown multimode properties relative to high speed VCSEL operation, and in particular have shown a simple rate equation analysis can be used to accurately predict the mode competition in a VCSEL.

The measured bit error rate (BER) for a VCSEL as a function of the received power is shown in Fig. 11. When all of the laser emission is coupled into the fiber, (polarizer at 0°) the laser BER performance is quite good, and follows normal Gaussian statistics. However, when the coupling into the fiber discriminates the various VCSEL modes, significant limitations on performance are introduced. The laser used for this study was lasing in two transverse modes, each orthogonally polarized. The action of the polarizer is then to selectively attenuate one of the modes. The BER degrades with increasing mode selective loss (polarizer at 15, 30, -15 and -30) until eventually, when one of the polarization is eliminated, (polarizer at -45°) an error floor is found at approximately

10 -9. Conversely, when the orthogonal mode is eliminated, (polarizer at +45) the error floor is approximately 10 -7. The worst case BER performance occurs when one of the modes is completely eliminated.

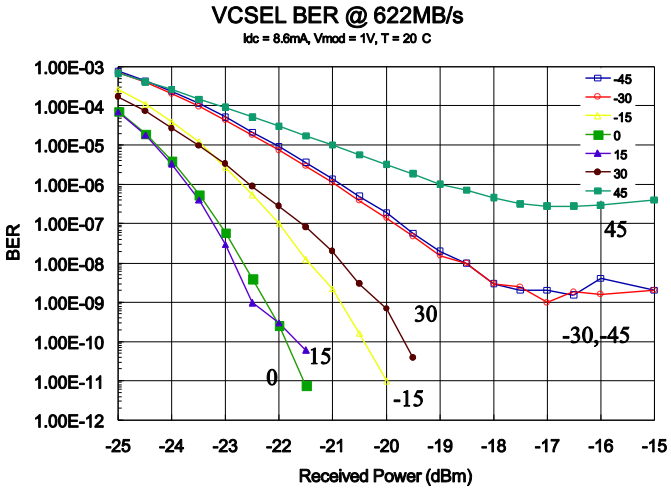

Figure 11. Measured BER with polarization selective coupling loss.

Figures 12, 13 and 14 show the accumulated noise on a long pulse when the polarizer is rotated to 0, -45, and +45 degrees respectively. The oscilloscope was placed in an infinite persistence mode, and the data was collected for ten minutes. In each case the total horizontal scale is 10ns, and total vertical scale is 750mV. In each of the figures, there is a histogram of the noise on the right hand side of the figure. The worst case BER performance coincides with a dramatic increase in the noise on the pulse when only one modes is selected, as shown in Figs 13 and 14. When both modes are passed equally as in Fig. 12, the noise disappears. Figures 13 and 14 also show the noise remains for long pulse durations, indicating the noise source is not simply turn on jitter. This means the optical power is being dynamically and randomly partitioned between the modes with the constraint that the total power remains constant, creating polarization mode partition noise. This should not be confused with the phenomenon of the same name observed in multilongitudinal mode edge emitting lasers in dispersive links. In that case the mechanism is the same but the modes are separated temporally by a long dispersive fiber link and thus create dispersion penalties. In our case, the modes are separated by only a few angstroms, there is no need for a long dispersive fiber link, and the modes are discriminated by polarization. The resultant effect is amplitude noise, which disappears when the polarizer is set to pass both modes equally, and increases as the polarizer is rotated to selectively block one of the modes.

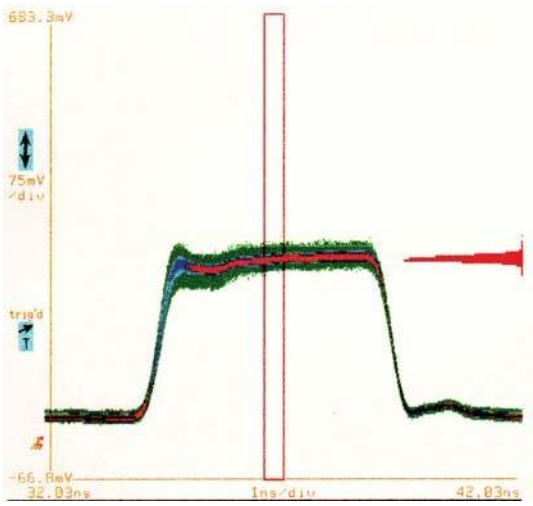

Figure 12. polarizer at 0 degrees.

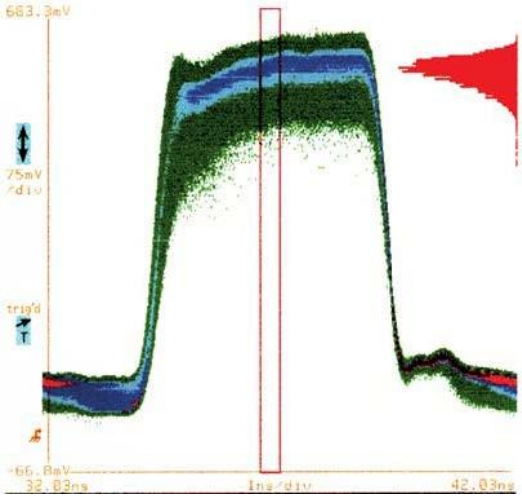

Figure 13. Polarizer at -45.

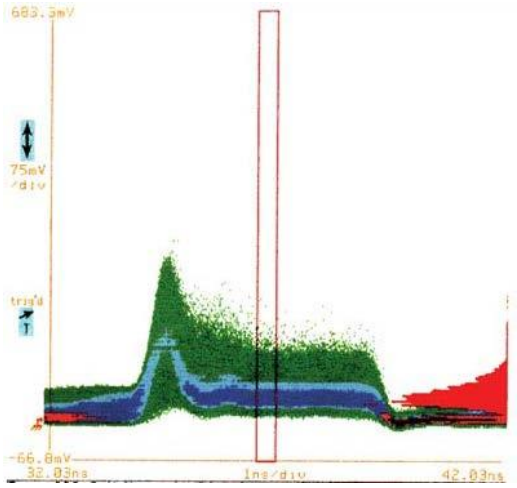

Figure 14. Polarizer at +45.

It should be noted that polarization mode partition noise will cause an error floor to arise, not simply a power penalty. The BER is set by the Signal to Noise Ratio (SNR) of the detected pulse. When the dominant noise source is receiver thermal noise, if there is a degradation of the pulse which causes an increase in BER, then the BER can be returned to its original value by increasing the amplitude of the signal. The amount of increase required is called the power penalty. By contrast, an error floor arises when no further increase in signal amplitude can restore the BER, and is the limiting BER performance of the link. In our case, an error floor results because the mode partitioning limits the maximum optical SNR before the receiver noise is even added. When the partitioning reduces the SNR of the optical signal below that required to maintain a certain BER, no further improvement in SNR can be obtained by increasing the amplitude of the optical signal. An error floor results because the noise increases proportionately to the pulse amplitude. When the polarizer passes both modes equally, then the partition noise will vanish because the total optical power is always being transmitted. The noise is worse on the rising edge of the pulse and then appears to improve slightly as the pulse settles to its steady state on-level. This is probably due to the laser turning on entirely in one mode or the other. If it turns on in the mode which does not pass through the polarizer, then the pulse will appear to remain at zero until the other mode turns on, creating turn-on delay. When the turn-on transient has decayed, however, the partition noise remains but the discrimination is only partial such that it never completely extinguishes either mode. The fact the total power remains constant suggests that what is happening from pulse to pulse is the distribution of power between the modes varies, but the total power is held constant due to gain saturation of the laser. It is not clear at this point whether the power in each mode remains constant for the duration of a pulse or whether it changes continuously, possibly driven by spontaneous emission.

CONCLUSIONS

We have presented an equivalent circuit model that is useful for designing high speed interfacing circuits to VCSELs. The model is quite simple, but yet robust in that it fits our measured data over a very broad range of operating characteristics. The differential carrier lifetime was extracted from our equivalent circuit, and was shown to vary with the bias current. For accurate calculations of the carrier density in the active region, the bias dependent carrier lifetime must be used. We have also identified some of the nuances of multi-transverse mode VCSELs for communications. In particular, we have shown that each of the modes may have a significantly different rise time, fall time and pulse shape. A relatively simple multimode rate equation model was used to predict the exact individual pulseshapes. The model is valid when there is signi-ficant spatial overlap of the individual modes in the gain volume, and each of the modes is competing for the same gain. The modal competition also produces significant effects from a systems point of view. When one of the lasing modes is selectively eliminated, the emission contains a large amount of polarization mode partitioning noise, and can be the limiting factor on BER performance. However, the polarization mode partitioning noise observed here is not the same effect observed with multi-longitudinal mode edge emitting lasers, and is completely eliminated by coupling all of the VCSEL emission into the fiber network.

References

[1] H. Q. Hoe, H. C. Chui, K. D. Choquette, B. E. Hammons, W. G. Breiland and K. M. Geib, “Highly Uniform and

Reproducible Vertical-Cavity Surface-Emitting Lasers Grown by Metalorganic Vapor Phase Epitaxy with a In Situ

Reflectometry,” IEEE Phot. Tech. Lett., vol. 8, pp. 1285-1287, 1996.

[2] J. K. Guenter, R. A. Hawthorne, D. N. Granville, M. K. Hibbs-Brenner and R.A. Morgan, “Reliability of Proton-

Implanted VCSELs for Data Communications,” Proc. SPIE vol. 2683, 1996.

[3] R. A. Morgan, M. K. Hibbs-Brenner, T. M. Marta, R. A. Walterson, S. Bounnak, E. L. Kalweit and J. A. Lehman,

“200°C, 96nm Wavelength Range, Continuous-Wave Lasing from Unbonded GaAs MOVPE-Grown Vertical Cavity

Surface Emitting Lasers,” IEEE Phot. Tech. Lett., vol. 7, pp. 441-443, 1995.

[4] G. E. Shtengal, D. A. Ackerman, and P. A. Morton, “True Carrier Lifetime Measurements of Semiconductor Lasers,”

Elect. Lett., vol. 31, pp. 1747-1748, 1995.

[5] A. K. Jansen van Doom, M. P. van Exter and J. P. Woerdman, “Elasto-optic Anisotropy and Polarization Orientation of

Vertical-Cavity Surface-Emitting Semiconductor Lasers,” Appl. Phys. Lett., vol. 69, pp. 1041-1043, 1996.

[6] H. Li, T. L. Lucas, J. G. McInerney and R. A. Morgan, “Modes and Patterns of Electrically Pumped Vertical-Cavity

Surface-Emitting Lasers,” Chaos, Solitons, and Fractals, vol. 4, pp. 1619-1636, 1994.

[7] A.E. Siegman, LASERS, University Science Books, Mill Valley, CA, 1986.

[8] K. D. Choquette and R. E. Leibenguth, “Control of Vertical-Cavity Laser Polarization with Anisotropic Transverse

Cavity Geometries,” IEEE Phot. Tech. Lett., vol. 6, pp. 40-42, 1994.

[9] J. Ser, Y. Ju, J. Shjin and Y. H. Lee, “Polarization Stabilization of Vertical-Cavity Top-Surface-Emitting Lasers by

Inscription of Fine Metal-Interlaced Gratings,” IEEE Phot. Tech. Lett., vol. 66, pp. 2769-2771, 1995.

[10] A . Chavez-Pirson, H. Ando, H. Saito and H. Kanbe, “Polarization Properties of a Vertical Cavity Surface Emitting

Laser Using a Fractional Layer Superlattice Gain Medium,” Appl. Phys. Lett., vol. 62, pp. 3082-3084, 1993.

[11] T . Numai, K. Kurihara, K. Kuhn, H. Kosaka. I. Ogura, M. Kajita, H. Saito and K. Kasahara, “Control of Light-Output

Polarization for Surface Emitting Laser Type Device by Strained Active Layer Grown on Misoriented Substrate,” IEEE

J. Quant. Elec., vol. 31, pp. 636-642, 1995.

[12] D . V. Kuksenkov, H. Temkin, and T. Yoshikawa, “Dynamic properties of Vertical Cavity Surface emitting Lasers with

Improved Polarization Stability,” IEEE Phot. Tech. Lett., vol. 8, pp. 977-979, 1996.

[13] D . Smith, “Characterizing Components for High Speed Data Interconnects,” Symposium on Optical Fiber

Measurements, Boulder, CO, October 1996.

[14] Y . Lam, J. P. Loehr, and J. Singh, “Comparison of Steady-State and Transient Characteristics of Lattice-Matched and

Strained InGaAS-AlGaAs (on GaAs) and InGasAS-AlInAs (on InP) Quantum-Well Lasers,” IEEE J. Quant. Elec., vol. 28, pp. 1248-1260, 1992.

[15] A . Valle, J. Sarma and K. A. Shore, “Spatial Holeburning Effects on the Dynamics of Vertical Cavity Surface-Emitting

Laser Diodes,” IEEE J. Quant. Elec., vol. 31, pp. 1423-1431, 1995.

[16] O . Buccafusca, J. L. A. Chilla, J. J. Rocca, S. Field, C. Wilmsen, V Morozov, and R, Leibenguth, “Transverse Mode

Dynamics in Vertical Cavity Surface Emitting Lasers Excited by Fast Electrical Pulses,” Appl. Phys. Lett., vol. 68, pp. 590-592, 1996.

ADVANCED OPTICAL COMPONENTS

Finisar’s ADVANCED OPTICAL COMPONENTS division was formed through strategic acquisition of key optical compon-ent suppliers. The company has led the industry in high volume Vertical Cavity Surface Emitting Laser (VCSEL) and associated detector technology since 1996. VCSELs have become the primary laser source for optical data communi-cation, and are rapidly expanding into a wide variety of sensor applications. VCSELs’ superior reliability, low drive current, high coupled power, narrow and circularly symmetric beam and versatile packaging options (including arrays) are enabling solutions not possible with other optical technologies. ADVANCED OPTICAL COMPONENTS is also a key supplier of Fabrey-Perot (FP) and Distributed Feedback (DFB) Lasers, and Optical Isolators (OI) for use in single mode fiber data and telecommunications networks

LOCATION

- Allen, TX - Business unit headquarters, VCSEL wafer growth, wafer fabrication and TO package assembly.
- Fremont, CA – Wafer growth and fabrication of 1310 to 1550nm FP and DFB lasers.
- Shanghai, PRC – Optical passives assembly, including optical isolators and splitters.

SALES AND SERVICE

Finisar’s ADVANCED OPTICAL COMPONENTS division serves its customers through a worldwide network of sales offices and distributors. For application assistance, current specifications, pricing or name of the nearest Authorized Distributor, contact a nearby sales office or call the number listed below.

AOC CAPABILITIES

ADVANCED OPTICAL COMPONENTS' advanced capabilities include:

- 1, 2, 4, 8, and 10Gbps serial VCSEL solutions
- 1, 2, 4, 8, and 10Gbps serial SW DETECTOR solutions
- VCSEL and detector arrays
- 1, 2, 4, 8, and 10Gbps FP and DFB solutions at 1310 and 1550nm
- 1, 2, 4, 8, and 10Gbps serial LW DETECTOR solutions
- Optical Isolators from 1260 to 1600nm range
- Laser packaging in TO46, TO56, and Optical subassemblies with SC, LC, and MU interfaces for communication networks
- VCSELs operating at 670nm, 780nm, 980nm, and 1310nm in development
- Sensor packages include surface mount, various plastics, chip on board, chipscale packages, etc.
- Custom packaging options

Contact Information

Finisar Corporation
1389 Moffett Park Drive
Sunnyvale, CA USA 94089
Phone: +1 (408) 548-1000
Email: sales@finisar.com
Website: www.finisar.com